Contributions of radiative gluons and vector mesons to the F_2 structure function

F. Zamani
Department of Physics, Villanova University, Villanova, Pennsylvania 19085, USA
(Received 12 December 2008; published 27 March 2009)

We calculate unpolarized quark distribution functions and F_2 structure functions for the proton and the neutron. The calculation is preformed in the light-cone frame. For the bare nucleon three different distributions—namely, spin-0 diquark, spin-0 plus spin-1 diquark, and no diquark models—have been used. Using perturbative QCD an initial gluon distribution is generated inside the core nucleon. The physical nucleon is assumed to be a superposition of the bare nucleon plus virtual light-cone Fock states of baryon octets and baryon decuplets along with the corresponding pseudoscalar mesons and vector mesons. The initial distributions are evolved. The F_2 structure functions are calculated from the evolved distributions and it is shown that they are in reasonable agreement with the NMC and ZEUS results along with a CTEQ6M fit. Also, it is shown that the meson cloud is a major contributing factor to the sea quark asymmetry and one needs both pseudoscalar mesons and vector mesons to account fully for Gottfried sum rule violation.

DOI: 10.1103/PhysRevC.79.035208 PACS number(s): 12.39.Ki, 14.20.Dh, 14.65.Bt, 24.85.+p

I. INTRODUCTION

The meson cloud model has been used extensively to investigate nucleon structure. It all started with Sullivan's original work in 1972 [1], which pointed to the significance of the pionic structure of the nucleon in high-energy processes. Sullivan examined the role of one-pion exchange (OPE) in deep inelastic scattering from nucleons. The pion being the lightest meson is expected to play a dominant role in the nucleon structure. Since the 1980s there have been numerous publications investigating the role that heavier mesons play in the nucleon structure [2–41]. In 1983 Thomas [10] realized that the pionic content of the nucleon broke the SU(3)-flavor symmetry. Thomas used the πNN process to put a limit on the hardness of the πNN form factor. In 1990 Henley and Miller [11] used the pion cloud to explain the asymmetry between $\bar{d}$ and $\bar{u}$. Kumano [12–14] used both πNN and $\pi N\Delta$ processes to put limits on the cutoff parameters for monopole, dipole, and exponential from factors and their effects on the flavor asymmetry of the sea quark. Kumano's [12] work showed that the upper limits for the cutoff mass should be 0.60, 0.95, and 0.75 GeV for monopole, dipole, and exponential form factors, respectively. In 1991 Hwang and collaborators [15] extended the analysis of deep inelastic lepton scattering data by taking into account the effects of additional mesons including ρ, ω, σ, K, and K^*. Their work suggested that the πNN and $\pi N\Delta$ from factors are harder than what was suggested by previous works. Namely, the cutoff masses, according to their calculations, are over 1000 MeV instead of being less than 500 MeV as suggested by previous works. In the early 1990s Schreiber and collaborators [18] used both πNN and $\pi N\Delta$ processes to calculate the nucleon structure functions in the bag model. In 1992 Zoller [17] used the Fock state decomposition of the nucleon in the light-cone frame to investigate the effects of soft pion exchange on the proton and neutron structure functions in deep inelastic lepton scattering. Holtmann, Speth, and collaborators have used a similar approach to investigate polarized and unpolarized nucleon structure functions [25,27,28,30]. Pasquini, Boffi, and collaborators have used the meson cloud to investigate generalized parton distributions [37–39] and the electroweak structure of the nucleon [40].

Before introducing the meson cloud one needs to start with the bare nucleon. For that we use the light-front formalism. Since the original work by Dirac [42] several decades ago, there has been an extensive use of the light-front frame to study high-energy processes. Among many other works, in the early 1990s Schlumpf [43,44] used this approach to investigate the electroweak properties of baryons. We used Schlumpf's approach to calculate the nucleon's F_2 and g_1 structure functions [2–6]. Miller has used the light-front formalism to investigate nucleon electromagnetic form factors [41]. Brodsky and collaborators have studied the spin and orbital angular momentum of composite systems in the light-cone frame [45]. For a more in-depth study of the subject the interested reader is referred to Refs. [46–49].

In Sec. II we briefly present a light-front representation of three-body systems and introduce the two types of wave functions that we will use for the core nucleon. This will be followed by the formalism for the meson cloud model in Sec. III. Results and discussion will be presented in Sec. IV, which will be followed by a summary in Sec. V.

II. LIGHT-FRONT REPRESENTATION OF THE NUCLEON

In the following we present the basic definitions and formalism [43,44]. A four-vector in the light-front frame is defined as

$$a = (a^+, a_-, a_\perp), \tag{1}$$

where $a^\pm = (a^0 \pm a^3)/\sqrt{2}$ and $a_\perp = (a^1, a^2)$. Following the relativistic treatment of the nucleon by Berestetskii and Terent'ev [50,51], we separate the center-of-mass motion of the three quarks in the nucleon from their relative motion by transforming their momenta, p_1, p_2, p_3, into total and relative

momenta as follows:

$$\vec{P} = \vec{p}_1 + \vec{p}_2 + \vec{p}_3, \tag{2a}$$

$$\xi = \frac{p_1^+}{p_1^+ + p_2^+}, \quad \eta = \frac{p_1^+ + p_2^+}{P^+}, \tag{2b}$$

$$q_\perp = (1-\xi)p_{1\perp} - \xi p_{2\perp}, \qquad Q_\perp = (1-\eta)(p_{1\perp} + p_{2\perp}) - \eta p_{3\perp}. \tag{2c}$$

Then, the Hamiltonian of the system takes the form

$$H = \frac{P_\perp^2 + \hat{M}^2}{2P^+}, \tag{3}$$

where $\hat{M}$ is the mass operator with the interaction term W:

$$\hat{M} = M + W, \tag{4a}$$

$$M^2 = \frac{Q_\perp^2}{\eta(1-\eta)} + \frac{M_3^2}{\eta} + \frac{m_3^2}{1-\eta}, \tag{4b}$$

$$M_3^2 = \frac{q_\perp^2}{\xi(1-\xi)} + \frac{m_1^2}{\xi} + \frac{m_3^2}{1-\xi}, \tag{4c}$$

with m_1, m_2, and m_3 as the constituent quarks masses. M and M_3 can be rewritten in a more transparent way in terms of the relative momenta q and Q:

$$E_1 = \sqrt{\mathbf{q}^2 + m_1^2}, \quad E_2 = \sqrt{\mathbf{q}^2 + m_2^2}, \quad E_3 = \sqrt{\mathbf{Q}^2 + m_3^2}, \quad E_{12} = \sqrt{\mathbf{Q}^2 + M_3^2}, \tag{5a}$$

$$\xi = \frac{E_1 + q_3}{E_1 + E_2}, \quad \eta = \frac{E_{12} + Q_3}{E_{12} + E_3}, \tag{5b}$$

$$M = E_{12} + E_3, \quad M_3 = E_1 + E_2, \tag{5c}$$

where $\mathbf{q} = (q_1, q_2, q_3)$ and $\mathbf{Q} = (Q_1, Q_2, Q_3)$.

The wave function of the nucleon can be written as

$$\Psi = \Phi\chi\phi, \tag{6}$$

where Φ, χ, and ϕ are the flavor, spin, and momentum distributions, respectively. We are going to consider two different wave functions for the core nucleon. First, assume that the nucleon is a quark-diquark system. In general, the nucleon state can be a linear combination of the spin-isospin diquark states (0, 0), (0, 1), (1, 0), and (1, 1) written as

$$\begin{aligned}\Psi_1 = {} & \frac{A}{\sqrt{2}}\big[uud\big(\chi^{\rho 1}\phi_1^{\lambda 1} + \chi^{\rho 2}\phi_1^{\lambda 2}\big) - udu\big(\chi^{\rho 1}\phi_1^{\lambda 1} - \chi^{\rho 3}\phi_1^{\lambda 3}\big) \\ & - duu\big(\chi^{\rho 2}\phi_1^{\lambda 2} + \chi^{\rho 3}\phi_1^{\lambda 3}\big)\big] \\ & + \frac{B}{\sqrt{6}}\big[uud\big(\chi^{\rho 1}\phi_1^{\rho 1} + \chi^{\rho 2}\phi_1^{\rho 2} - 2\chi^{\rho 3}\phi_1^{\rho 3}\big) \\ & + udu\big(\chi^{\rho 1}\phi_1^{\rho 1} - 2\chi^{\rho 2}\phi_1^{\rho 2} + \chi^{\rho 3}\phi_1^{\rho 3}\big) \\ & + duu\big(-2\chi^{\rho 1}\phi_1^{\rho 1} + \chi^{\rho 2}\phi_1^{\rho 2} + \chi^{\rho 3}\phi_1^{\rho 3}\big)\big] \\ & + \frac{C}{\sqrt{2}}\big[uud\big(\chi^{\lambda 1}\phi_1^{\rho 1} + \chi^{\lambda 2}\phi_1^{\rho 2}\big) \\ & - udu\big(\chi^{\lambda 1}\phi_1^{\rho 1} - \chi^{\lambda 3}\phi_1^{\rho 3}\big) - duu\big(\chi^{\lambda 2}\phi_1^{\rho 2} + \chi^{\lambda 3}\phi_1^{\rho 3}\big)\big] \\ & + \frac{D}{\sqrt{6}}\big[uud\big(\chi^{\lambda 1}\phi_1^{\lambda 1} + \chi^{\lambda 2}\phi_1^{\lambda 2} - 2\chi^{\lambda 3}\phi_1^{\lambda 3}\big) \\ & + udu\big(\chi^{\lambda 1}\phi_1^{\lambda 1} - 2\chi^{\lambda 2}\phi_1^{\lambda 2} + \chi^{\lambda 3}\phi_1^{\lambda 3}\big) \\ & + duu\big(-2\chi^{\lambda 1}\phi_1^{\lambda 1} + \chi^{\lambda 2}\phi_1^{\lambda 2} + \chi^{\lambda 3}\phi_1^{\lambda 3}\big)\big].\end{aligned} \tag{7a}$$

For the second case we assume that there is no clustering of the quarks inside the nucleon [43]:

$$\Psi_2 = \frac{-1}{\sqrt{3}}(uud\chi^{\lambda 3} + udu\chi^{\lambda 2} + duu\chi^{\lambda 1})\phi_2. \tag{7b}$$

We will be using three wave functions called Set 1, Set 2, and Set 3. Set 1 and Set 2 correspond to the models that we have used in Refs. [2–6]. Set 1 is the spin-0 diquark with $A = 0.9798$, $B = -0.2$, $C = 0.0$, and $D = 0.0$ in Eq. (7a). Set 2 is Eq. (7b). Set 3 is the model used in Ref. [2] that includes the spin-1 diquark with $A = -0.7874$, $B = 0.0$, $C = 0.0$, and $D = -0.6164$ in Eq. (7a). Also, in Eq. (7), u and d represent the up and down flavor, and χ^{ρ_i} and χ^{λ_i} with $i = 1, 2, 3$ represent the Melosh transformed spin wave functions [52], for example,

$$\chi_\uparrow^{\rho 3} = \frac{1}{\sqrt{2}}(\uparrow\downarrow\uparrow - \downarrow\uparrow\uparrow), \tag{8a}$$

$$\chi_\downarrow^{\rho 3} = \frac{1}{\sqrt{2}}(\uparrow\downarrow\downarrow - \downarrow\uparrow\downarrow), \tag{8b}$$

$$\chi_\uparrow^{\lambda 3} = \frac{1}{\sqrt{6}}(\downarrow\uparrow\uparrow + \uparrow\downarrow\uparrow - 2\uparrow\uparrow\downarrow), \tag{8c}$$

$$\chi_\downarrow^{\lambda 3} = \frac{1}{\sqrt{6}}(2\downarrow\downarrow\uparrow - \downarrow\uparrow\downarrow - \uparrow\downarrow\downarrow). \tag{8d}$$

The spin wave function of the ith quark is

$$\uparrow = R_i\begin{pmatrix}1\\0\end{pmatrix}, \quad \downarrow = R_i\begin{pmatrix}0\\1\end{pmatrix}. \tag{9}$$

In Eq. (9), R_i are the Melosh matrices:

$$R_1 = \frac{1}{\sqrt{a^2 + Q_\perp^2}\sqrt{c^2 + q_\perp^2}} \times \begin{pmatrix} ac - q_R Q_L & -aq_L - cQ_L \\ cQ_R + aq_R & ac - q_L Q_R \end{pmatrix}, \tag{10a}$$

$$R_2 = \frac{1}{\sqrt{a^2 + Q_\perp^2}\sqrt{d^2 + q_\perp^2}} \times \begin{pmatrix} ad + q_R Q_L & -aq_L - dQ_L \\ dQ_R - aq_R & ad - q_L Q_R \end{pmatrix}, \tag{10b}$$

$$R_3 = \frac{1}{\sqrt{b^2 + Q_\perp^2}}\begin{pmatrix} b & Q_L \\ -Q_R & b \end{pmatrix}, \tag{10c}$$

where

$$a = M_3 + \eta M, \quad b = m_3 + (1-\eta)M, \tag{11a}$$

$$c = m_1 + \xi M_3, \quad d = m_2 + (1-\xi)M_3, \tag{11b}$$

$$q_R = q_1 + iq_2, \quad q_L = q_1 - iq_2, \tag{11c}$$

$$Q_R = Q_1 + iQ_2, \quad Q_L = Q_1 - iQ_2. \tag{11d}$$

The functions $\phi_1^{\rho i}$ and $\phi_1^{\lambda i}$, with $i = 1, 2, 3$, and ϕ_2 are the momentum wave functions, which we take to be of the

following form:

$$\phi_1^{\rho i} = N_{\rho i}(X_j - X_k)\phi_1^{si}/X_T, \tag{12a}$$

$$\phi_1^{\lambda i} = N_{\lambda i}(X_j + X_k - 2X_i)\phi_1^{si}/X_T, \tag{12b}$$

with $i \neq j \neq k$, and [43]

$$\phi_2 = \frac{N}{(M^2+\beta^2)^{3.5}}. \tag{12c}$$

Also,

$$X_3 = \frac{Q_\perp^2}{2\eta(1-\eta)\beta_Q^2} + \frac{q_\perp^2}{2\eta\xi(1-\xi)\beta_q^2} + \frac{m_1^2}{2\eta\xi\beta_q^2} + \frac{m_2^2}{2\eta(1-\xi)\beta_q^2} + \frac{m_3^2}{2(1-\eta)\beta_Q^2}, \tag{13a}$$

$$X_2 = q_\perp^2 \frac{(1-\eta)(1-\xi)\beta_Q^2 + \xi\beta_q^2}{2\beta_Q^2\beta_q^2\eta\xi(1-\xi)(1-\eta+\xi\eta)} + Q_\perp^2 \frac{(1-\xi)(1-\eta)\beta_q^2 + \xi\beta_Q^2}{2\beta_Q^2\beta_q^2\eta(1-\eta)(1-\eta+\xi\eta)} + q_\perp Q_\perp \frac{\beta_Q^2 - \beta_q^2}{\beta_Q^2\beta_q^2\eta(1-\eta+\xi\eta)} + \frac{m_1^2}{2\eta\xi\beta_q^2} + \frac{m_2^2}{2\eta(1-\xi)\beta_Q^2} + \frac{m_3^2}{2(1-\eta)\beta_q^2}, \tag{13b}$$

$$X_1 = q_\perp^2 \frac{(1-\xi)\beta_q^2 + \xi(1-\eta)\beta_Q^2}{2\beta_Q^2\beta_q^2\eta\xi(1-\xi)(1-\xi\eta)} + Q_\perp^2 \frac{(1-\xi)\beta_Q^2 + \xi(1-\eta)\beta_q^2}{2\beta_Q^2\beta_q^2\eta(1-\xi)(1-\xi\eta)} - q_\perp Q_\perp \frac{\beta_Q^2 - \beta_q^2}{\beta_Q^2\beta_q^2\eta(1-\xi\eta)} + \frac{m_1^2}{2\eta\xi\beta_Q^2} + \frac{m_2^2}{2\eta(1-\xi)\beta_q^2} + \frac{m_3^2}{2(1-\eta)\beta_q^2}, \tag{13c}$$

$$X_T = X_1 + X_2 + X_3, \tag{13d}$$

and

$$\phi_1^{si} = \frac{1}{(1+X_T)^{ni}}. \tag{13e}$$

In these equations β_Q, β_q, and β are confinement scale parameters and $N_{\rho_i}, N_{\lambda_i}$, and N are normalization constants.

III. MESON CLOUD MODEL IN THE LIGHT-CONE FRAME

Using the convolution model, one can decompose the physical nucleon in terms of the core nucleon and intermediate, virtual meson-baryon states [2–6,25,27,28,30]:

$$|N\rangle = Z^{1/2}[|N\rangle_{\text{bare}} + \sum_{BM} \beta_{BM}|BM\rangle], \tag{14}$$

where Z is the probability of the physical nucleon being in the core state, BM stands for a virtual baryon-meson state, and β_{BM} is the probability amplitude for the physical nucleon being in the BM state. The summation in Eq. (14), in general, includes all physically possible pairs from the meson octet and baryon octet and decuplet. In terms of the quark distributions one can write

$$q_N(x) = Z\left[q_{N,\text{core}}(x) + \sum_{MB}\alpha_{MB}\left(\int_x^1 n_{MB}(y)q_M\left(\frac{x}{y}\right)\frac{dy}{y} + \int_x^1 n_{BM}(y)q_B\left(\frac{x}{y}\right)\frac{dy}{y}\right)\right], \tag{15}$$

where x is the fraction of the total momentum of the nucleon being carried by the quark, q, α_{MB} are spin-flavor Clebsch-Gordan coefficients, n_{MB} and n_{BM}, the splitting functions, are the probabilities of the nucleon being in state of MB or BM, respectively, and y is the fraction of the momentum being carried by the meson (baryon) in $n_{MB}(y)$ [$n_{BM}(y)$]. The splitting functions must satisfy the following equations:

$$n_{MB}(y) = n_{BM}(1-y) \tag{16}$$

and

$$\langle x n_{MB}\rangle + \langle x n_{BM}\rangle = \langle n_{BM}\rangle. \tag{17}$$

In Eq. (17) $\langle n\rangle$ and $\langle xn\rangle$ are the first and second moments of the splitting functions. Equation (16) ensures the global charge conservation and Eq. (17) momentum conservation.

To calculate $q_N(x)$ one needs to know $q_{N,\text{core}}(x)$, $q_M(x), q_B(x)$, and $n_{MB}(x)$ explicitly. To calculate the core quark distribution we use the following expression [53]:

$$q_{i,\text{core}}(x) = \int [dx][dk_\perp]\delta(x_i - x)|\phi(x_i, k\perp i)|^2, \tag{18}$$

with

$$[dx] = \frac{dx_1\,dx_2\,dx_3}{\sqrt{(x_1x_2x_3)}}, \quad [dk_\perp] = dk_{\perp 1}dk_{\perp 2}, \quad \sum_i x_i = 1, \quad \sum_i k_{\perp i} = 0, \tag{19}$$

where $x_1 = \xi\eta, x_2 = \eta(1-\xi)$, and $x_3 = 1-\eta$. For ϕ in Eq. (18) we use the expression in Eq. (12). We calculate $q_M(x)$ in the following way [54]:

$$q_M(x) = \frac{1}{4}\int \frac{dk_\perp}{x(1-x)} M_0(x,k_\perp)|\Phi_\pi(x,k_\perp)|^2, \tag{20a}$$

where

$$M_0^2(x,k_\perp) = \frac{k_\perp^2 + m_q^2}{x(1-x)}, \tag{20b}$$

$$\Phi_\pi(x,k_\perp) = Ne^{\frac{-k^2}{(2\Lambda_\pi)^2}}, \tag{20c}$$

and

$$k^2 = \left(k_\perp^2/4 + (x-1/2)^2 m_q^2\right)/x(1-x). \tag{20d}$$

$q_B(x)$ is calculated using the core distributions. To calculate $n_{MB}(x)$ we use [17,28,30]

$$n_{MB}(y) = \frac{g_{NMB}^2}{16\pi^2}\frac{1}{y^2(1-y)}\int_0^\infty dk_\perp^2 \frac{\left|\Gamma_{MB}\left(M_{MB}^2\right)\right|^2}{\left(M_{MB}^2 - m_N^2\right)^2} \times [(m_B - ym_N)^2 + \mathbf{k}_\perp^2], \tag{21a}$$

for pseudoscalar meson-baryon octet intermediate states, and

$$n_{MB}(y) = \frac{g_{NMB}^2}{16\pi^2}\frac{1}{6m_B^2 y^4(1-y)}\int_0^\infty dk_\perp^2 \frac{\left|\Gamma_{MB}\left(M_{MB}^2\right)\right|^2}{\left(M_{MB}^2 - m_N^2\right)^2} \times [(m_B + y m_N)^2 + \mathbf{k}_\perp^2]^2[(m_B - y m_N)^2 + \mathbf{k}_\perp^2], \tag{21b}$$

for pseudoscalar meson-baryon decuplet intermediate states. We have evaluated the splitting functions for vector meson-baryon octet pairs as

$$\begin{aligned} n_{MB}(y) = {} & \frac{1}{64\pi^2 m_M^2}\frac{1}{y^4(1-y)^2}\int_0^\infty dk_\perp^2 \frac{\left|\Gamma_{MB}\left(M_{MB}^2\right)\right|^2}{\left(M_{MB}^2 - m_N^2\right)^2} \\ & \times \Big(f_{NMB}^2\big(4m_M^4 y^2((1-y)^2(m_B - m_N y)^2 \\ & + (1+y)^2\mathbf{k}_\perp^2) + 4\big((1-y)\big(m_B^2 - m_N^2 y\big) + \mathbf{k}_\perp^2\big)^2 \\ & \times \big((1-y)^2(m_B - m_N y)^2 \\ & + 8m_M^2 y((1-y)^2(m_B - m_N)^2(8m_B m_N y \\ & + m_N^2(5-y)y - m_B^2(1-5y)\big) \\ & + (1-y)(10m_B m_N(1-y)y \\ & - m_N^2(5-y)y(1-2y) + m_B^2(2-y)(1-5y))\mathbf{k}_\perp^2 \\ & - (1-(6-y)y)\mathbf{k}_\perp^4\big)\big)\big) + f_{NMB}g_{NMB} \\ & \times (4m_M^4(1-y)y^3(m_B - m_N y) \\ & + 4(1-y)y\big((1-y)\big(m_B^2 - m_N^2 y\big) - \mathbf{k}_\perp^2\big) \\ & \times (m_B m_N(1-y)^2(m_B - m_N y) \\ & - (m_B + 2m_B y - m_N(2+y))\mathbf{k}_\perp^2\big) \\ & + 4m_M^2(1-y)y^2(-9(m_B - m_N) \\ & \times (1-y)(m_B - m_N y)^2 - 2(m_N(5-4y) \\ & + m_B(4-5y)\mathbf{k}_\perp^2)\big)\big) + g_{NMB}^2\big(m_M^4 y^4 \\ & + 2m_m^2 y^2\big((1-y)^2 + \big(4m_B^2 - 9m_B m_N y + 4m_N^2 y^2\big) \\ & + (4 - y(1-4y))\mathbf{k}_\perp^2\big) + y^2\big(m_B^2 m_N^2(1-y)^4 \\ & + 2\big(2m_B^2 - 3m_B m_N + 2m_N^2\big)(1-y)^2 y^2 + y^4\big)\big)\big) \end{aligned} \tag{22a}$$

and vector meson-baryon decuplet pairs as

$$\begin{aligned} n_{MB}(y) = {} & \frac{f_{NMB}^2}{48\pi^2}\frac{1}{y(1-y)} \\ & \times \int_0^\infty dk_\perp^2 \frac{\left|\Gamma_{MB}\left(M_{MB}^2\right)\right|^2}{\left(M_{MB}^2 - m_N^2\right)^2}\frac{1}{6m_B^2 y^3(1-y)^2} \\ & \times \big(m_B^4(y-1)^4\big(m_B^2 + 3m_N^2 y^2 \\ & + m_B^2(y-1)^2(3 + y(-2+3y))\big)\mathbf{k}_\perp^2 \\ & + \big(m_N^2 y^2 + m_B^2\big(3 + 4(y-1)y\big)\big)\mathbf{k}_\perp^2 + \mathbf{k}_\perp^6 \\ & + m_M^4 y^4\big(3m_B^2 + m_N^2 y^2 + \mathbf{k}_\perp^2\big) \\ & + 2m_M^2 y^2\big(m_B^2(y-1)^2\big(m + B^2 - 6m_B m_N + m_N^2 y^2\big) \\ & + \big(m + B^2 - 6m_B m_N + m_n^2 y^2\big) \\ & + \big(m_N^2 y^2 + m_B^2(y^2-1)\big)\mathbf{k}_\perp^2 + \mathbf{k}_\perp^4\big)\big). \end{aligned} \tag{22b}$$

In Eqs. (20) and (21), $\Gamma(M_{MB}^2)$ is the vertex form factor, which is parametrized by the exponential function of the invariant mass, M_{MB}, of the intermediate baryon-meson state:

$$\Gamma\left(M_{MB}^2\right) = e^{-\frac{\left(M_{MB}^2 - m_N^2\right)}{\Lambda_{MB}^2}}, \tag{23}$$

with Λ_{MB} as free parameters, which are determined by fitting experimental data. Putting all these pieces together and using all possible intermediate baryon-meson states one could calculate the physical quark distributions in the proton and the neutron. In the current work we use pseudoscalar mesons, vector mesons, baryon octet and decuplet intermediate states. These initial distributions are calculated at some initial low value of Q_0^2. To be able to compare our results with experiments, we evolve these initial distributions using Dokshitzer, Gribov, Lipatov, Altarelli and Parisi (DGLAP) equations [55–57] to some final high Q^2. The DGLAP equations are

$$\frac{dq^i(x,t)}{dt} = \frac{\alpha(t)}{2\pi}\int_x^1 \frac{dy}{y}\left[\sum_{j=1}^{2f} q^j(y,t)P_{q^i q^j}\left(\frac{x}{y}\right) + G(y,t)P_{q^i G}\left(\frac{x}{y}\right)\right], \tag{24a}$$

$$\frac{dG(x,t)}{dt} = \frac{\alpha(t)}{2\pi}\int_x^1 \frac{dy}{y}\left[\sum_{j=1}^{2f} q^j(y,t)P_{Gq^j}\left(\frac{x}{y}\right) + G(y,t)P_{GG}\left(\frac{x}{y}\right)\right], \tag{24b}$$

for singlet distributions, and

$$\frac{dq^{NS}(x,t)}{dt} = \frac{\alpha(t)}{2\pi}\int_x^1 \frac{dy}{y} q^{NS}(y,t)P^{NS}\left(\frac{x}{y}\right), \tag{24c}$$

for nonsinglet distributions. In Eq. (24) α is the QCD running coupling constant, q and G are the quark and gluon distribution functions, P's are the splitting functions, f is the number of flavors, t is defined as [56]

$$t = \ln\left(Q^2/Q_0^2\right), \tag{24d}$$

and $\alpha(t)$ in the leading logarithmic approximation is of the form

$$\frac{\alpha(0)}{\alpha(t)} = 1 + b\alpha(0)t, \tag{24e}$$

where b is a constant [56]. Having the distribution functions one can calculate the nucleon structure functions from

$$2F_1 = F_2/x = \sum_i^f e_i^2[q^i(x) + \bar{q}^i(x)], \tag{25}$$

where e_i is the charge of the ith quark.

IV. RESULTS AND DISCUSSION

In Table I we present the parameters, in energy units of GeV, that have been used in Eqs. (13), (12), (16), and (17) to calculate quark distribution functions and the proton

TABLE I. Parameters used in Sets 1, 2, and 3. Here m_u, m_d, β_Q, and β_q are all in GeV, and μ_p and μ_n are in nuclear magneton units. Set 1 and Set 3 represent our diquark-quark models; Set 2 represents parameters used by Schlumpf [43,44].

	m_u	m_d	β_Q	β_q	n_1	n_2	n_3	μ_p	μ_n
Set 1	0.250	0.210	0.25	0.45	2.8	2.8	2.6	2.82	−1.61
Set 2	0.263	0.263	0.607	0.607	3.5	3.5	3.5	2.81	−1.66
Set 3	0.250	0.210	0.25	0.45	2.8	2.8	2.6	2.79	−1.68

and neutron structure functions. Set 1 represents the spin-0 diquark distribution for the core nucleon. Set 2 comprises the parameters used by Schlumpf [43] and represents a symmetrical distribution of quarks inside the nucleon. Set 3 is a superposition of spin-0 and spin-1 diquark wave functions. In our calculations we have used three other sets, identified as Set 1g, Set 2g, and Set 3g. These sets are identical to Set 1, Set 2, and Set 3 in all respects except for the presence of gluons in the initial distributions before the introduction of the meson cloud. We use the work done by Barone and collaborators [58] to build up a gluon distribution inside the nucleon. In this approach one starts with the bare nucleon and builds the gluon distribution in small increments of Q^2 (the details of which are presented in the Appendix). In Fig. 1 we show the gradual change in the Set 3 u-quark distribution from bare nucleon to the final state of $Q^2 = 0.5$ GeV^2. The total number of gluons at this stage turns out to be about six and they carry around 27% of the nucleon's momentum. We should add that the motivation for introducing gluons is to make it possible for the quark model to reproduce the F_2 structure function that agrees with observation [59].

For the cutoff parameters we have used a universal value of 0.880 GeV for all vertices. This numerical value is well within the acceptable range as shown in the introduction. For the coupling constants we choose [17,60] $\frac{g^2_{p\pi^0 p}}{4\pi} = 13.6$ and $\frac{g^2_{p\Delta^{++}\pi^-}}{4\pi} = 10.85$ GeV^{-2}. Other coupling constants are related to these two through the quark model [30,60,61].

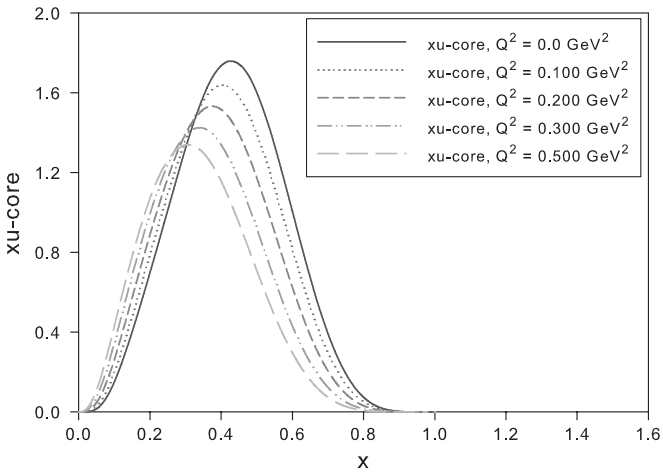

FIG. 1. xu-core distributions for Set 3 at different Q^2 values, as gluons are built up inside the nucleon.

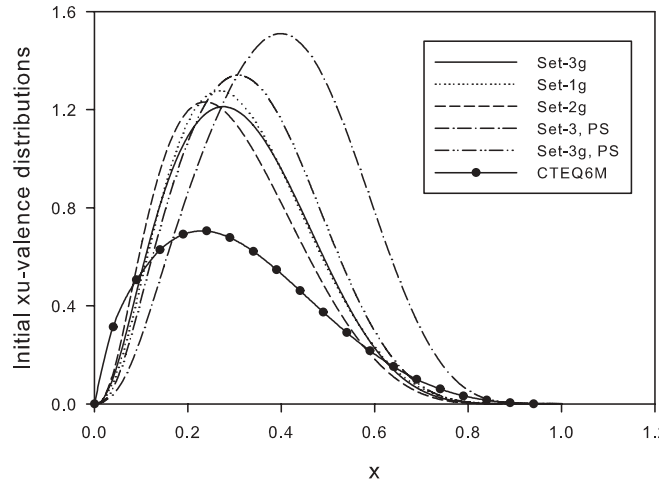

FIG. 2. Initial xu-valence distributions for Set 3g (spin-0 and spin-1 diquark), Set 1g (only spin-0 diquark), Set 2g (no diquark), Set 3, PS (no initial gluons and no vector mesons; only pseudoscalar mesons), Set 3g, PS (no vector mesons; only pseudoscalar mesons), and CTEQ6M.

Starting at the initial momentum transferred the quark distributions are evolved using the code by Miyama and Kumano [62] to final momentum transferred and compared with NMC [63,64] and ZEUS [65–67] results and the CTEQ6M fit [68]. The code uses the $\bar{M}S$ renormalization scheme and calculates Q^2 evolution to the next-to-leading order (NLO) of running coupling constant using brute-force numerical integration. Some of the input parameters are the initial and final momentum transferred squared, the QCD scale parameter, and the number of flavors, which can be three or four. Table II presents the initial momentum transferred squared and QCD scale parameter for our work, NMC, ZEUS, and CTEQ6M. The NMC data are reproduced using Eq. (2) in Ref. [64]. The ZEUS data are reproduced using the ZEUS-S QCD NLO fit [65,66]. To generate the CTEQ6M results we have used their Λ_{5f}, where $5f$ means five flavors. However, our value is more in line with Λ_{4f}, as is shown in Table II. All initial distributions are evolved to the final momentum transferred of 70 GeV^2. In Figs. 2 and 3 we present our initial xu-valence and xd-valence quark distributions for the three models and compare them with the corresponding CTEQ6M distributions [68]. A few points need to be made here. In our previous work we established the fact that the introduction of the gluons improves the distributions considerably [2]. Our current result shows that the addition of vector mesons to the meson cloud modifies the distributions significantly. For example, this can be observed in Fig. 2, by comparing

TABLE II. Initial momentum transferred squared and QCD scale parameter for this work, NMC [62,63], ZEUS [64,65], CTEQ6M four-flavor, and CTEQ6M five-flavor [67].

	This work	NMC	ZEUS	CTEQ6M-4f	CTEQ6M-5f
Q_0^2 (GeV^2)	0.50	20.0	7.0	1.69	1.69
Λ (GeV)	0.318	0.250	0.255	0.326	0.226

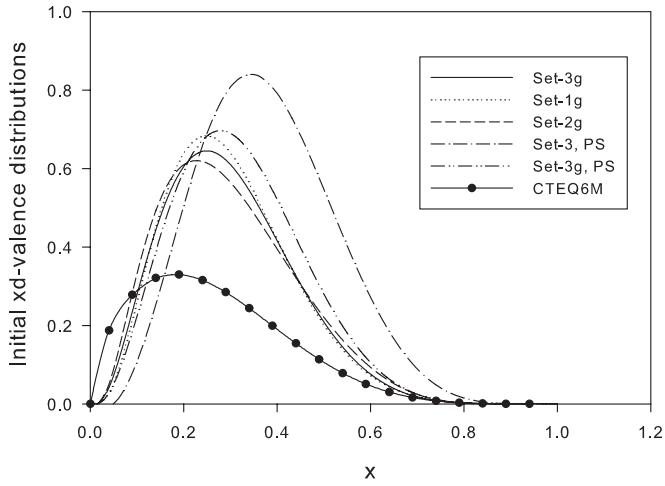

FIG. 3. Initial xd-valence distributions for Set 3g (spin-0 and spin-1 diquark), Set 1g (only spin-0 diquark), Set 2g (no diquark), Set 3, PS (no initial gluons and no vector mesons; only pseudoscalar mesons), Set 3g, PS (no vector mesons; only pseudoscalar mesons), and CTEQ6M.

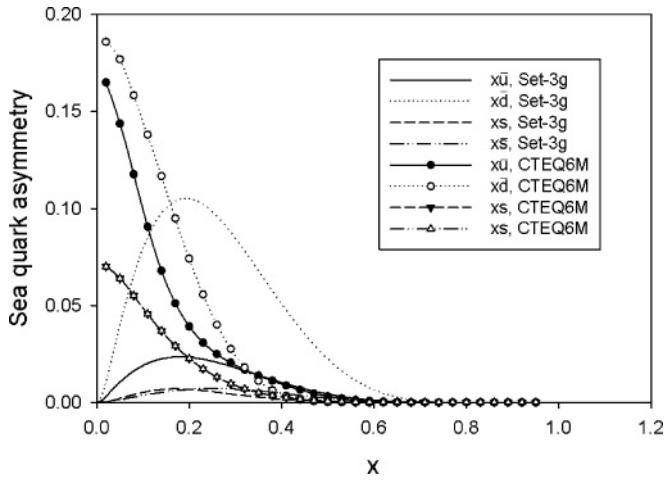

FIG. 4. Sea quark asymmetry resulting from the meson cloud for Set 3g (spin-0 and spin-1 diquark) and CTEQ6M.

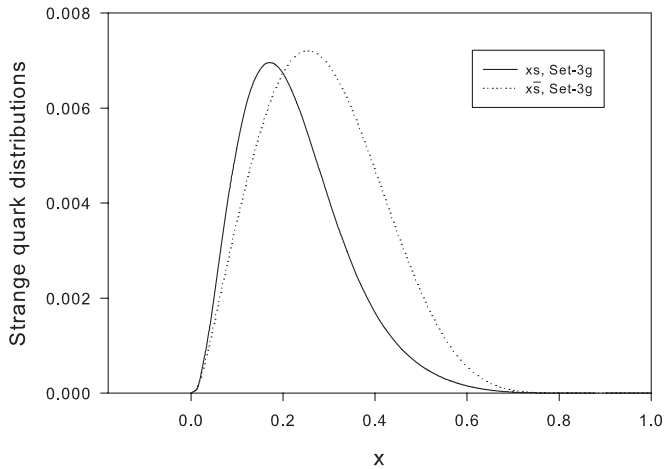

FIG. 5. Strange quark asymmetry resulting from the meson cloud for Set 3g (spin-0 and spin-1 diquark).

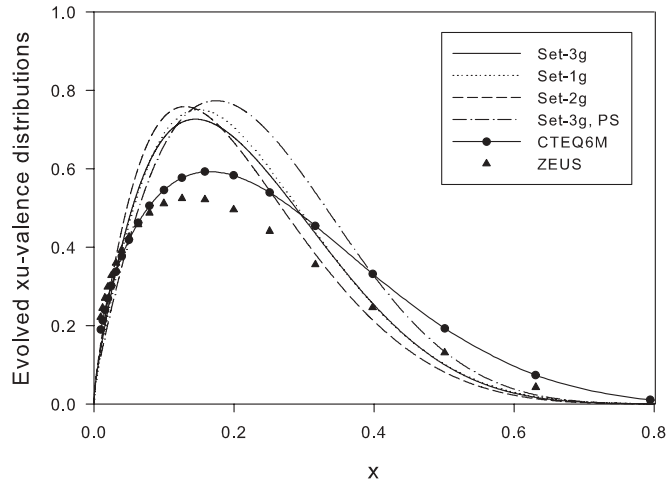

FIG. 6. Evolved xu-valence distributions for Set 3g (spin-0 and spin-1 diquark), Set 1g (only spin-0 diquark), Set 2g (no diquark), Set 3g, PS (no vector mesons; only pseudoscalar mesons), CTEQ6M, and ZEUS.

Set 3g and Set 3g PS with CTEQ6M. Also, the Set 2g u-valence distribution is lower than those of the diquark models from $x \geqslant 0.3$ to $x \sim 0.7$. The same is true, to a lesser degree, for d-valence distributions in the range $x \geqslant 0.2$ to $x \sim 0.5$. This is why the structure function calculated using Set 2 undershoots observation for the aforementioned range of x to a higher degree and therefore the nucleon with no diquark is not as suitable a model as one with a diquark for our purpose. In Fig. 4 we present the sea quark asymmetry generated by pseudoscalar and vector mesons and their corresponding baryons. Our results show that the meson cloud does indeed play a role as a source of sea quark asymmetry. However, the CTEQ6M data peak at much lower x. One point has to be made about the strange quarks: In the CETQ6M fit, the strange quark distribution is assumed to be the same as the antistrange quark distribution. However, in reality we know that that is not the

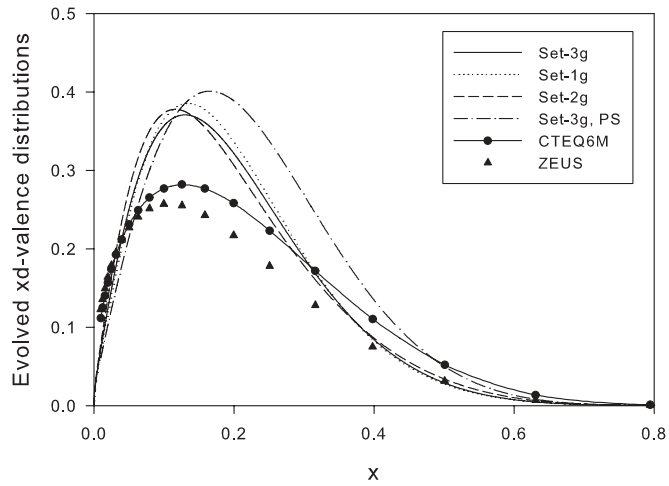

FIG. 7. Evolved xd-valence distributions for Set 3g (spin-0 and spin-1 diquark), Set 1g (only spin-0 diquark), Set 2g (no diquark), Set 3g, PS (no vector mesons; only pseudoscalar mesons), CTEQ6M, and ZEUS.

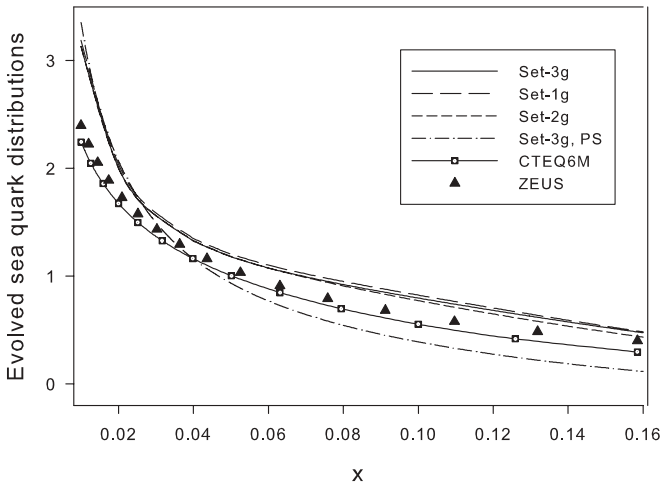

FIG. 8. Evolved sea quark distributions for Set 3g (spin-0 and spin-1 diquark), Set 1g (only spin-0 diquark), Set 2g (no diquark), Set 3g, PS (no vector mesons; only pseudoscalar mesons), CTEQ6M, and ZEUS.

case and our results in Fig. 5 do indeed show the strange quark asymmetry. Of course, the net strangeness inside the nucleon is zero and in our case $\int_0^1 [s(x) - \bar{s}(x)]dx \sim 10^{-4} \sim 0$. We evolve the initial distributions to $Q_f^2 = 70\ \text{GeV}^2$. Having seen the important role of the gluons in the distribution functions, from now on we will consider only those data sets. The results for xu valence and xd valence are shown in Figs. 6 and 7. As expected, there is a shift to lower x for the distributions. Also, the differences between our models and CTEQ6M and ZEUS have been reduced noticeably, particularly for Set 3g. For $x \geqslant 0.5$, there is a rather good agreement between both diquark models and the ZEUS result. Figures 8 and 9 compare the sea quark and gluon distributions of our models with ZEUS and CTEQ6M. For the sea quark distribution, the addition of the vector mesons has resulted in our distributions, for

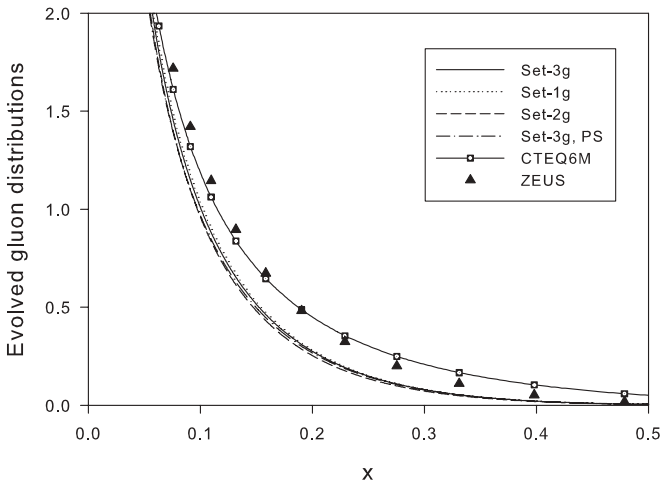

FIG. 9. Evolved gluon distributions for Set 3g (spin-0 and spin-1 diquark), Set 1g (only spin-0 diquark), Set 2g (no diquark), Set 3g, PS (no vector mesons; only pseudoscalar mesons), CTEQ6M, and ZEUS.

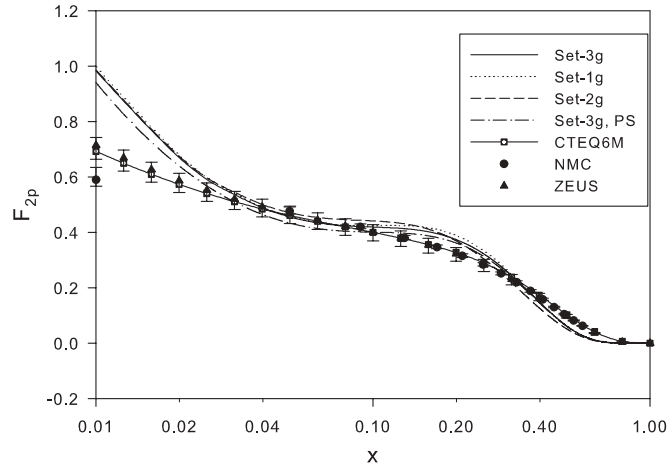

FIG. 10. F_2 structure function for the proton. The curves are the results of our models Set 3g (spin-0 and spin-1 diquark), Set 1g (only spin-0 diquark), Set 2g (no diquark), and Set 3g, PS (no vector mesons; only pseudoscalar mesons). Circles and triangles are NMC and ZEUS fits, respectively, at $Q^2 = 70\ \text{GeV}^2$. The curve with the open square symbol is the CTEQ6M fit.

$x \geqslant 0.04$, from being slightly less than CTEQ6M and ZEUS to being slightly more. For $x \leqslant 0.02$, all three models overshoot observation. For gluons, our models are consistently less than CTEQ6M and ZEUS data. For $x \geqslant 0.05$, Set 3g is closest to the CTEQ6M and ZEUS whereas Set 2g has the largest difference.

We use the final quark distributions to calculate the F_2 structure functions for the proton and the neutron. Figures 10 and 11 show the structure functions F_2 for the proton and the neutron, respectively. In both cases the three models are within the ZEUS error bar range all the way down to $x \sim 0.02$. Between $x = 0.02$ and $x = 0.1$ our F_{2p} has a better agreement with data compared with F_{2n}. Also, in the same

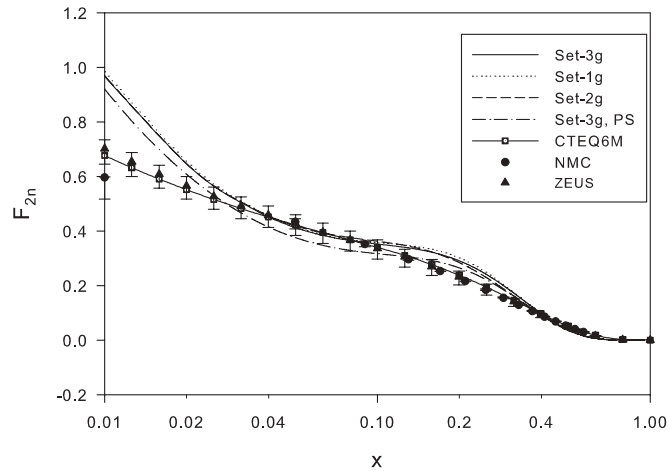

FIG. 11. F_2 structure function for the neutron. The curves are the results of our models Set 3g (spin-0 and spin-1 diquark), Set 1g (only spin-0 diquark), Set 2g (no diquark), and Set 3g, PS (no vector mesons; only pseudoscalar mesons). Circles and triangles are NMC and ZEUS fits, respectively, at $Q^2 = 70\ \text{GeV}^2$. The curve with the open square symbol is the CTEQ6M fit.

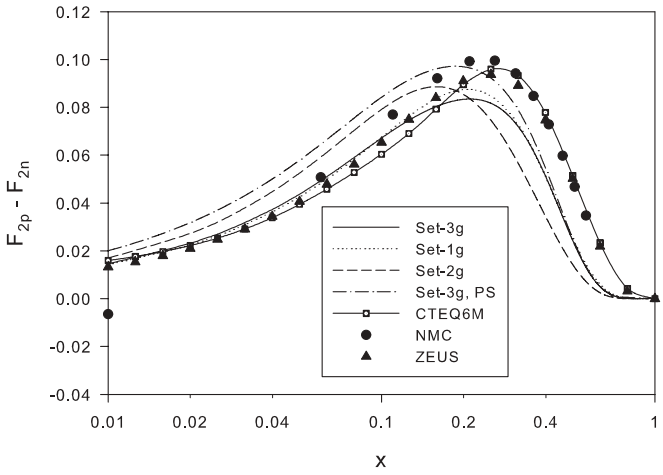

FIG. 12. Difference in proton and neutron F_2 structure functions. The curves are the results of our models Set 3g (spin-0 and spin-1 diquark), Set 1g (only spin-0 diquark), Set 2g (no diquark), and Set 3g, PS (no vector mesons; only pseudoscalar mesons). Circles and triangles are NMC and ZEUS fits, respectively, at $Q^2 = 70$ GeV^2. The curve with the open square symbol is the CTEQ6M fit.

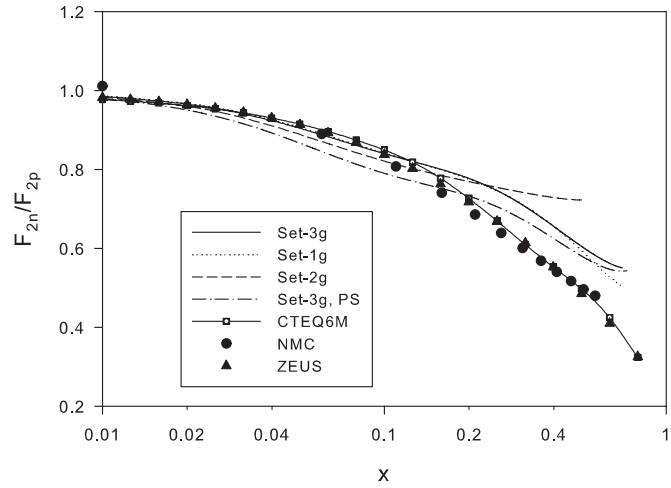

FIG. 13. Ratio of the neutron to proton F_2 structure functions. The curves are the results of our models Set 3g (spin-0 and spin-1 diquark), Set 1g (only spin-0 diquark), Set 2g (no diquark), and Set 3g, PS (no vector mesons; only pseudoscalar mesons). Circles and triangles are NMC and ZEUS fits, respectively, at $Q^2 = 70$ GeV^2. The curve with the open square symbol is the CTEQ6M fit.

range, inclusion of the vector mesons improves the agreement of our models with observation. For $x > 0.1$, the situation is reversed. For $x \leqslant 0.02$, our results diverge from data rather significantly, indicating that the model is not suitable for that range. Figures 12 and 13 show $F_{2p} - F_{2n}$ and F_{2n}/F_{2p}, respectively. These two graphs demonstrate clearly not only that the diquark models are indeed in better agreement with observation than the case in which there is no diquark but also that inclusion of vector mesons (Set 3g) has led to an excellent agreement with observation for $x < 0.2$.

In the quark model, the Gottfried sum rule (GSR) [69] can be written as

$$\int_0^1 \frac{dx}{x}[F_{2p}(x, Q^2) - F_{2n}(x, Q^2)] = \frac{1}{3}. \tag{26}$$

NMC [70,71] results show deviations from the right-hand side of Eq. (26):

$$\int_0^1 \frac{dx}{x}[F_{2p}(x, 4\ \text{GeV}^2) - F_{2n}(x, 4\ \text{GeV}^2)] = 0.240 \pm 0.0034 \pm 0.021. \tag{27}$$

This deviation can be attributed to the flavor asymmetry of the nucleon sea. In Table III, we present GSR results for our models, NMC, ZEUS, and CTEQ6M at $Q^2 = 70\,\text{GeV}^2$. For NMC and ZEUS calculations we have used their parametrizations and integrated over x from zero to one. Therefore, one can conclude that the contribution of pseudoscalar mesons and vector mesons is necessary and sufficient to reproduce the observed flavor asymmetry.

TABLE III. GSR results for this work, NMC [62], ZEUS [64,65], and CTEQ6M five-flavor [67] at $Q^2 = 70$ GeV^2.

	Set 3g	Set 2g	Set 1g	Set 3g, PS	NMC	ZEUS	CTEQ6M-5f
GSR	0.207	0.209	0.219	0.265	0.212	0.232	0.236

V. SUMMARY

We used a quark-diquark model for the bare nucleon. We considered two different diquark distributions, one with only spin-0 diquarks and the other a superposition of spin-0 and spin-1 diquarks. Using a perturbative QCD approach we generated gluons in the core nucleon before the addition of the meson cloud. It turned out that the addition of vector mesons to the meson cloud led to a better agreement between our models and NMC and ZEUS results for the proton and the neutron F_2 structure functions for the lower values of x. However, at higher x values the pseudoscalar meson cloud is in better agreement with observation. For the difference and the ratio of the proton and neutron structure functions the introduction of the vector mesons to the meson cloud leads to excellent agreement with observation for $x < 0.2$. We have shown that the meson cloud model is a source of sea quark asymmetry and one needs both pseudoscalar mesons and vector mesons to account fully for the Gottfried sum rule violation. Therefore, the introduction of gluons made it possible for our model to not only account for the GSR violation but also have a reasonable agreement with experimental observation of F_2 structure functions.

APPENDIX

Following the work done by Barone and collaborators [58], one can consider a transition $v(x) \to q(x) + g(x)$, where $v(x)$ is the initial valence quark distribution in the quark model and $g(x)$ is the gluon distribution generated in the process. Knowing $v(x)$, one can calculate $q(x)$ and $g(x)$ in the following

way:

$$q(x, Q_1^2) = v(x)\left[1 - \int_0^1 dy G(1-y, Q_1^2, 0)\right] + \int_x^1 \frac{dy}{y} G(1-y, Q_1^2, 0)\left[v\left(\frac{x}{y}\right) - yv(x)\right], \tag{A1}$$

$$\tilde{g}(x, Q_1^2, 0) = \int_x^1 \frac{dy}{y} v\left(\frac{x}{y}\right) G(y, Q_1^2, 0), \tag{A2}$$

where $G(x, Q_1^2, 0)$ is the flux of gluons generated from the target quark,

$$G(x, Q_1^2, 0) = \frac{4}{3}\int_0^{Q_1^2} d^2\vec{k}\frac{\alpha_s(\vec{k}^2)}{2\pi} V(-k_g^2) \times \frac{\left([1+(1-x)^2]\vec{k}^2 + x^4 m_f^2\right)}{x\left[\vec{k}^2 + (1-x)\mu_G^2 + x^2 m_f^2\right]^2}, \tag{A3}$$

with the gluon's virtuality given by

$$-k_g^2 = \frac{\vec{k}^2 + x^2 m_f^2}{(1-x)}, \tag{A4}$$

$V(\vec{k})$ as the vertex function related to the charge form factor of the nucleon,

$$V(\vec{k}) = 1 - F_{\text{charge}}(3\vec{k}^2), \tag{A5}$$

m_f as the mass of the quark with flavor f, and μ_G as the effective mass of gluons, introduces so that the color forces do not propagate beyond the confinement radius and is taken to be about 145 MeV.

To perform the next step of evolution from Q_1^2 to Q_2^2 ($Q_2^2 > Q_1^2$), one repeats this procedure by replacing $v(x) \to q(x, Q_1^2)$ and $G(x, Q_1^2, 0) \to G(x, Q_2^2, Q_1^2)$, which leads to the new gluon distribution

$$g(x, Q_2^2) = \tilde{g}(x, Q_2^2, Q_1^2) + \tilde{g}(x, Q_1^2, 0), \tag{A6}$$

and obviously these along with Eq. (A1) will lead to $q(x, Q_2^2)$. This procedure can be repeated in small steps until one reaches the desired final Q^2, which in our case is 0.5 GeV^2. At this momentum transfer we introduce the meson cloud and evolve the distributions to the final momentum transfer.

[1] J. D. Sullivan, Phys. Rev. D **5**, 1732 (1972).
[2] F. Zamani, Phys. Rev. C **74**, 035204 (2006).
[3] F. Zamani, Nucl. Phys. **A755**, 365 (2005).
[4] F. Zamani, Phys. Rev. C **68**, 055202 (2003).
[5] F. Zamani and D. Saranchak, Phys. Rev. C **63**, 065202 (2001).
[6] F. Zamani, Phys. Rev. C **58**, 3641 (1998).
[7] A. W. Thomas, Nucl. Phys. **A518**, 186 (1990).
[8] S. Kumano, Phys. Rev. D **41**, 195 (1990).
[9] A. W. Thomas and G. A. Miller, Phys. Rev. D **43**, 288 (1991).
[10] A. W. Thomas, Phys. Lett. **B126**, 97 (1983).
[11] E. M. Henley and G. A. Miller, Phys. Lett. **B251**, 453 (1990).
[12] S. Kumano, Phys. Rev. D **43**, 59 (1991).
[13] S. Kumano, Phys. Rev. D **43**, 3067 (1991).
[14] S. Kumano and J. T. Londergan, Phys. Rev. D **44**, 717 (1991).
[15] W. Y. P. Hwang, J. Speth, and G. E. Brown, Z. Phys. A **339**, 383 (1991).
[16] W. Melnitchouk, A. W. Thomas, and A. I. Signal, Z. Phys. A **340**, 85 (1991).
[17] V. R. Zoller, Z. Phys. C **53**, 443 (1992).
[18] A. W. Schreiber, P. J. Mulders, A. I. Signal, and A. W. Thomas, Phys. Rev. D **45**, 3069 (1992).
[19] W. Y. P. Hwang and J. Speth, Phys. Rev. D **46**, 1198 (1992).
[20] A. W. Thomas and W. Melnitchouk, *New Frontiers in Nuclear Physics* (World Scientific, Singapore, 1993), p. 41.
[21] A. Szczurek and J. Speth, Nucl. Phys. **A555**, 249 (1993).
[22] A. Szczurek, J. Speth, and G. T. Garvey, Nucl. Phys. **A570**, 765 (1994).
[23] N. N. Nikolaev, A. Szczurek, J. Speth, and V. R. Zoller, Z. Phys. A **349**, 59 (1994).
[24] B. C. Pearce, J. Speth, and A. Szczurek, Phys. Rep. **242**, 193 (1994).
[25] F. M. Steffens, H. Holtmann, and A. W. Thomas, Phys. Lett. **B358**, 139 (1995).
[26] W. Melnitchouk and A. W. Thomas, Z. Phys. A **353**, 311 (1995).
[27] A. Szczurek, M. Ericson, H. Holtmann, and J. Speth, Nucl. Phys. **A596**, 397 (1996).
[28] J. Speth and A. W. Thomas, Adv. Nucl. Phys. **24**, 83 (1997).
[29] A. Szczurek, A. J. Buchmann, and A. Faessler, J. Phys. G **22**, 1741 (1996).
[30] H. Holtmann, A. Szczurek, and J. Speth, Nucl. Phys. **A596**, 631 (1996).
[31] S. J. Brodsky and B.-Q. Ma, Phys. Lett. **B381**, 371 (1996).
[32] W. Koepf, L. L. Frankfurt, and M. Strikman, Phys. Rev. D **53**, 2586 (1996).
[33] F. M. Steffens and A. W. Thomas, Phys. Rev. C **55**, 900 (1997).
[34] S. D. Bass and D. Schutte, Z. Phys. A **357**, 85 (1997).
[35] S. Kumano, Phys. Rep. **303**, 183 (1998).
[36] F. S. Navarra, M. Nielsen, and S. Paiva, Phys. Rev. D **56**, 3041 (1997).
[37] B. Pasquini and S. Boffi, Nucl. Phys. **A782**, 86 (2007).
[38] B. Pasquini and S. Boffi, Phys. Rev. D **73**, 094001 (2006).
[39] S. Boffi and B. Pasquini, Riv. Nuovo Cimento **30**, 387 (2007).
[40] B. Pasquini and S. Boffi, Phys. Rev. D **76**, 074011 (2007).
[41] G. A. Miller, Phys. Rev. C **66**, 032201(R) (2002).
[42] P. A. M. Dirac, Rev. Mod. Phys. **21**, 392 (1949).
[43] F. Schlumpf, Ph.D. thesis (University of Zurich, 1992).
[44] F. Schlumpf, Phys. Rev. D **47**, 4114 (1993).
[45] S. J. Brodsky, D. S. Hwang, B. Q. Ma, and I. Schmidt, Nucl. Phys. **B593**, 311 (2001).
[46] H. Leutwyler and J. Stern, Ann. Phys. (NY) **112**, 94 (1978).
[47] M. G. Fuda, Ann. Phys. (NY) **197**, 265 (1990).
[48] M. G. Fuda, Ann. Phys. (NY) **231**, 1 (1994).
[49] M. Burkardt, Adv. Nucl. Phys. **23**, 1 (1996).
[50] V. B. Berestetskii and M. V. Terent'ev, Sov. J. Nucl. Phys. **24**, 547 (1976).
[51] V. B. Berestetskii and M. V. Terent'ev, Sov. J. Nucl. Phys. **25**, 347 (1977).
[52] H. J. Melosh, Phys. Rev. D **9**, 1095 (1974).

[53] Z. Dziembowski, C. J. Martoff, and P. Zyla, Phys. Rev. D **50**, 5613 (1994).
[54] C. M. Shakin and W.-D. Sun, Phys. Rev. C **53**, 3152 (1996).
[55] V. N. Gribov and L. N. Lipatov, Sov. J. Nucl. Phys. **15**, 438 (1972).
[56] G. Altarelli and G. Parisi, Nucl. Phys. **B126**, 298 (1977).
[57] Yu. L. Dokshitzer, Sov. Phys. JETP **46**, 641 (1977).
[58] V. Barone, M. Genovese, N. N. Nikolaev, E. Predazzi, and B. G. Zakharov, Int. J. Mod. Phys. A **8**, 2779 (1993).
[59] J. Kuti and V. F. Weisskopf, Phys. Rev. D **4**, 3418 (1971).
[60] B. Holzenkamp, K. Holinde, and J. Speth, Nucl. Phys. **A500**, 485 (1989).
[61] G. E. Brown and W. Weise, Phys. Rep. **22**, 279 (1975).
[62] M. Miyama and S. Kumano, Comput. Phys. Commun. **94**, 185 (1996).
[63] P. Amaudruz *et al.*, Phys. Lett. **B295**, 166 (1992).
[64] M. Arneodo *et al.*, Phys. Lett. **B364**, 107 (1995).
[65] J. Rautenberg, Ph.D. thesis (University of Bonn, 2004).
[66] S. Chekanov *et al.*, Phys. Rev. D **67**, 012007 (2003).
[67] S. Chekanov *et al.*, Eur. Phys. J. C **21**, 443 (2001).
[68] J. Pumplin, D. R. Stump, J. Huston, H. L. Lai, P. Nadolsky, and W. K. Tung, J. High Energy Phys. 07 (2002) 012.
[69] K. Gottfried, Phys. Rev. Lett. **18**, 1174 (1967).
[70] P. Amaudruz *et al.*, Phys. Rev. Lett. **66**, 2712 (1991).
[71] M. Arneodo *et al.*, Phys. Rev. D **50**, R1 (1994).